Article

Dynamically Programmable Magnetic Fields for Controlled Movement of Cells Loaded with Iron Oxide Nanoparticles

Alex Pai, Pengpeng Cao, Ethan E White, Brian Hong, Torkom Pailevanian, Michelle Wang, Behnam Badie, Ali Hajimiri, and Jacob M. Berlin

ACS Appl. Bio Mater., **Just Accepted Manuscript** • DOI: 10.1021/acsabm.0c00226 • Publication Date (Web): 28 May 2020

Dynamically Programmable Magnetic Fields for Controlled Movement of Cells Loaded with Iron Oxide Nanoparticles

Alex Pai[†], Pengpeng Cao[‡], Ethan E. White[‡,§], Brian Hong[†], Torkom Pailevanian[†], Michelle Wang[†], Behnam Badie[‖,]*, Ali Hajimiri[†,]*, Jacob M. Berlin[‡,§,]*

[†] Department of Electrical Engineering, California Institute of Technology

[‡] Department of Molecular Medicine, City of Hope Beckman Research Institute

[§] Irell & Manella Graduate School of Biological Sciences, City of Hope

Department of Surgery, Division of Neurosurgery, City of Hope Beckman Research Institute

* Principal Investigators (J. Berlin, Ali Hajimiri, and B. Badie contributed equally.)

Corresponding Authors

Behnam Badie
Professor
Division of Neurosurgery
1500 East Duarte Road
Duarte, CA 91010
Phone: 626-471-7100
Fax: 626-471-7344
Email: bbadie@coh.org

Ali Hajimiri
Bren Professor of Electrical Engineering and Medical Engineering
Division of Engineering and Applied Science
1200 East California Boulevard
Pasadena, CA 91125
Phone: 626-395-2239
Email: hajimiri@caltech.edu

Jacob Berlin
Email: jacobberlincoh@gmail.com

Keywords

CAR T-cell, dynamically-programmable magnetic field, immunotherapy, iron-oxide nanoparticles, macrophage, magnetic transport, neural stem cell

ABSTRACT

Cell-based therapies are becoming increasingly prominent in numerous medical contexts, particularly in regenerative medicine and the treatment of cancer. However, since the efficacy of the therapy is largely dependent on the concentration of therapeutic cells at the treatment area, a major challenge associated with cell-based therapies is the ability to move and localize therapeutic cells within the body. In this Article, a technique based on dynamically programmable magnetic fields (DPMF) is successfully demonstrated to non-invasively aggregate therapeutic cells at a desired location. Various types of immune cells (neural stem cells, monocytes/macrophages, and CAR T-cells) are loaded with iron-oxide nanoparticles and then focused at a particular site using externally controlled electromagnets. These experimental results serve as a readily scalable prototype for the design of apparatuses that patients can wear which focus therapeutic cells at the anatomical sites needed for treatment.

INTRODUCTION

In recent years, there has been an increased interest in cell-based therapies. From regenerative medicine utilizing stem cells such as neural stem cells (NSCs) to cancer therapy utilizing chimeric antigen receptor (CAR) T-cells and macrophages, cell-based therapies are an expanding part of the therapeutic approach to a number of diseases.[1-9] A common theme among this diverse repertoire of cell therapies is the importance of localization. Whether trying to heal an infarct site or treat a brain tumor, the efficacy of the therapy is largely dependent on the ability of the cell product to reach and be retained at a specific anatomical site. Currently, this site-specific localization is generally achieved by a local injection or by relying on cell-intrinsic homing mechanisms.[4, 10, 11] However, these localization strategies are inefficient, and typically only a portion of the injected cell product is retained at the desired tissue site.[10, 11] Therefore, strategies that exert additional external control over cell localization could improve the efficacy of cell-based therapies.

Magnetic targeting is an emerging strategy for controlling cell localization. This general approach has been used in a number of applications and has been shown to alter cell localization both *in vitro* and *in vivo* without affecting cell viability.[12-21] For nearly all magnetic targeting studies, cells are loaded *ex vivo* with superparamagnetic iron oxide nanoparticles (IONPs) in order to make them responsive to magnetic fields. A number of different IONP formulations have been used for magnetic targeting studies, with no clear consensus on what types of particles are best and few head-to-head comparisons between different formulations.[16] Despite this variability in the types of IONPs used, these formulations are typically internalized inside the cells to achieve effective magnetic targeting.

The vast majority of previous studies, including our previous work on iron oxide-loaded immune cells,[17] have employed permanent magnets to direct cell accumulation.[13] This approach has clear drawbacks for focusing the accumulation of cells at a position within the body. A primary challenge is that no energetic minimums can exist in a volume containing no magnetic elements—this is known as Earnshaw's Theorem.[22] Therefore, magnetic material cannot be localized to a fixed position in the body using static external magnets. Implanted magnets create minimum energy wells at the target site but are invasive.

However, Earnshaw's theorem only applies to static magnetic fields. Using dynamically changing magnetic fields, energetic minimums can be obtained. Thus, work in this area has focused on using electromagnets which can easily create adjustable fields, but typically have lower fields due to power and cooling requirements. Programmable magnetic resonance imaging (MRI) using open-loop control for fine movement is one approach that has shown proof-of-principle, although this solution requires a customized MRI instrument and would likely be prohibitively expensive for the days-long timescale expected to be necessary for cell localization in humans. Rapidly pulsing strong electromagnets have also shown promise for targeting nanoparticle accumulation to a focal point in their center.[23] While this work illustrated the potential of this approach, it is uncertain if it could be extended to iron oxide-loaded cells as rapid magnetic field pulsing is known to cause iron oxide nanoparticles to heat their local environment.[24] Indeed, this strategy is being actively pursued for cancer therapy where the iron nanoparticles are localized to tumors and then a rapidly alternating magnetic field is applied.[25] In addition, given the size of the magnets used in this work, it is difficult to envision how this system could be applied to a multi-day application in humans.

Ideally, patients could be equipped with a wearable device that allows for programmable magnetic control over the course of days, and the fields applied would be non-toxic to the loaded

cells. Here we demonstrate an initial prototype of the key component to such a system: a miniaturized, flexible chip that allows for fine control of magnetically loaded cells using dynamically programmable magnetic fields (DPMF). This prototype has an active area of 16 mm^2, consisting of a flexible polymer with 8 individually controllable wires in both the horizontal and vertical directions overlapping in an electronic mesh grid. Because each wire is individually addressable, this system allows for millions of unique settings from which to generate unique fields and forces. Here, we demonstrate that *in vitro* this system can control the 2D accumulation at resolutions below 300 μm with no toxicity to the cells. The location of accumulation can be switched multiple times. This was demonstrated using three different cells types currently used in cell therapies: neural stem cells (NSCs), monocytes (THP-1), and chimeric antigen receptor (CAR) T-cells. In order to optimally load these cells with iron nanoparticles, two different coatings were used—NSCs and THP-1 cells endocytosed PEGylated iron-oxide nanoparticles, but CAR T-cells did not and instead were loaded by using silica-coated IONPs that stuck to the cell membrane. While the DPMF prototype is quite small, the device is passively cooled and the design can be directly scaled to larger areas. To the best of our knowledge, this work is the first to demonstrate a miniaturized device capable of rapidly programmable magnetic control of human cell movement.

RESULTS AND DISCUSSION

We previously developed an apparatus that allows for live cell imaging while a magnetic field is applied and used it to show that when immune cells are loaded with immunostimulatory IONPs the cells can be accumulated by applying a fixed permanent magnet.[17, 26] Here we used this system to evaluate our DPMF chip. The cell-box apparatus consists of a disposable, 3D-printable chassis that fits in a 100 mm petri dish (Figure 1a). A coverslip is affixed to the central region of the chassis and the DPMF chip is inserted to be flush against the backside of the coverslip. The assembled apparatus is then placed in a petri dish containing IONP-loaded cells and cell media. The chassis contains atmosphere distribution channels that allow for atmospheric regulation of the cell media and risers that keep the coverslip suspended just above the bottom of the petri dish.

The DPMF system is capable of over 1 million unique magnetic profiles within a 16 mm^2 active area.[17, 26] Controller circuitry (Figure 1b) is housed separately and electrically connects to the active area. The active area is passively cooled via a copper heatsink behind the active area. The active area is thermally connected to the copper attachment using thermal paste. As a demonstration of the aggregating ability of system, magnetic particles are moved to two different locations (Figure 1c). The particles (Bangs Laboratories, Indiana, USA) are magnetic microspheres large enough for visibility under microscopy (3 μm). The full video can be seen in Supplementary Video 1.

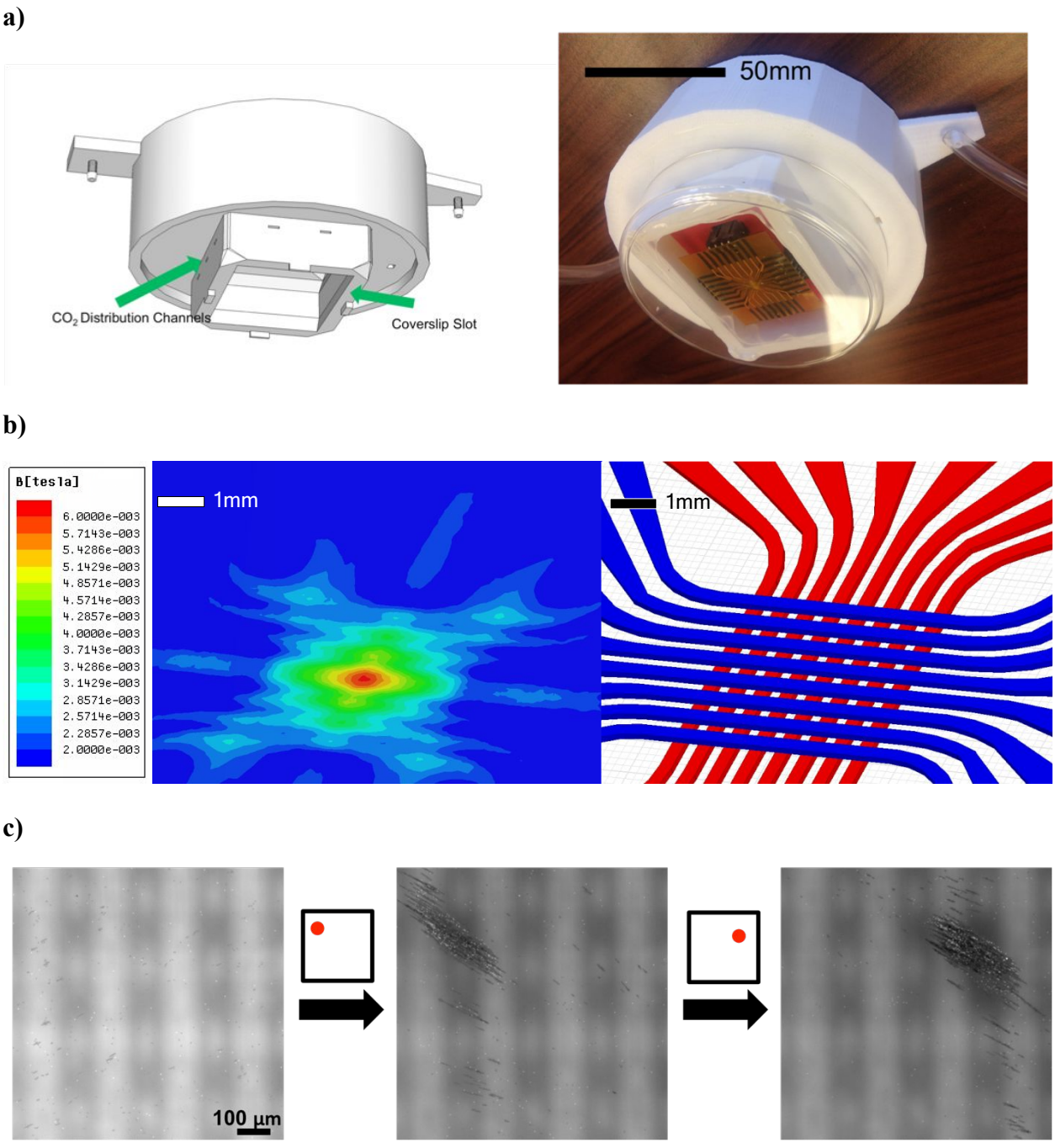

Figure 1. (a) Design of cell-box apparatus for imaging during DPMF. (b) A sample field profile for aggregating cells to a single point (left) and schema of the active area of the DPMF chip (right). (c) Positive control experiment. Magnetic particles 3 µm in diameter are used to verify the magnetic aggregation capabilities of the system.

Here, two types of surface modification chemistries (PEGylation by intercalation and silica-coating IONPs) were used to convert hydrophobic oleic acid-coated IONPs to hydrophilic, biocompatible IONPs prior to loading onto cells (Figure 2a). Following purification by centrifugation and washing, successful surface functionalization was confirmed by TEM, DLS,

zeta potential, and by the particles being readily dispersible in water (Figure 2b-c). The PEGylated particles (DSPE-IONP) showed an increase in hydrodynamic diameter from 30 to 98.2 nm and a relatively neutral zeta potential of -3.67, both of which are common for PEGylated particles. The Si-IONPs had a hydrodynamic diameter of 160 nm, a zeta potential of -16.56, and a coating visible in TEM images.

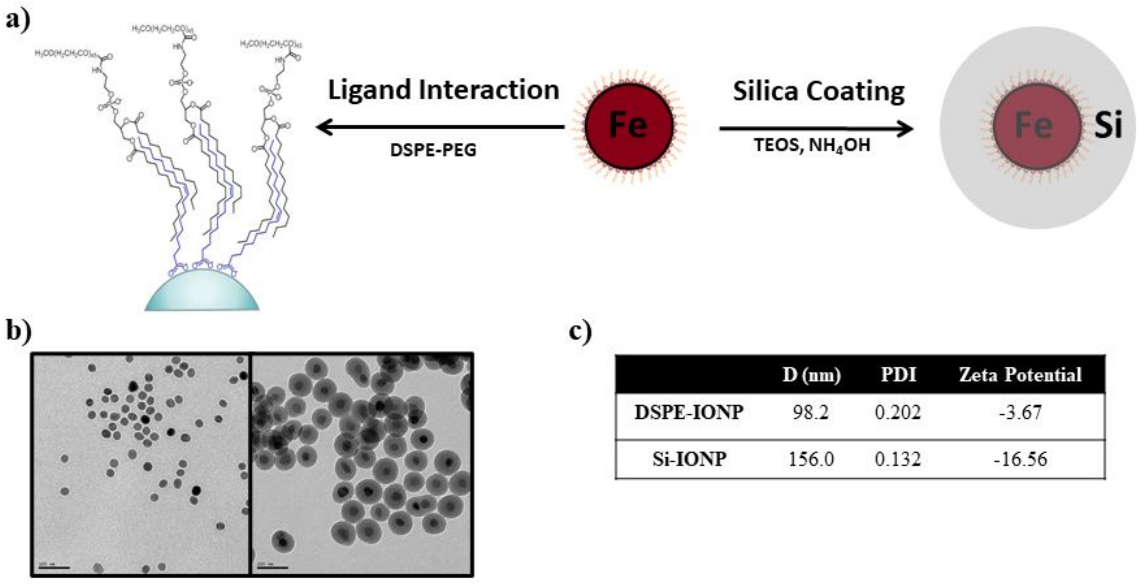

	D (nm)	PDI	Zeta Potential
DSPE-IONP	98.2	0.202	-3.67
Si-IONP	156.0	0.132	-16.56

Figure 2. Synthesis and characterization of DSPE-IONPs and Si-IONPs. Synthetic scheme of (a) DSPE-PEG-coated IONPs (DSPE-IONPs) and silica-coated IONPs (Si-IONPs). (b) TEM images of DSPE-IONPs and Si-IONPs. The scale bars in each image are 100 nm. (c) Table of the diameter, polydisperity index (PDI), and zeta potential of DSPE-IONPs and Si-IONPs.

In order to determine what IONP concentrations could be tolerated by cells, each IONP formulation was screened for cell toxicity (Figure 3b). Because this is a proof-of-principle study focused on the development of DPMF, we were primarily concerned about ensuring that the cells remained intact (e.g., minimal necrosis and cell debris) during the course of the *in vitro* experiments. Thus, the cells were evaluated for acute toxicity after 1 h of incubation with the IONPs. In general, it was found that doses at or above 45 µg were toxic to cells.

To confirm internalization of the IONPs, cells were incubated with 10 µg and loading was evaluated by TEM imaging (Figure 3a, Supplementary Figure 1). The Si-IONPs are readily identified by their distinctive fish-egg like structure with the dark iron core and lighter silica coating (Supplementary Figure 1a-e). However, the DSPE-NPs are more challenging to identify as they only possess a dark iron core and transparent polymer coating, so they are most readily identified as dark aggregates of unusual shape (Supplementary Figure 1f-i). It was found that the NSCs and THP-1 cells readily endocytosed IONPs (especially DSPE-IONPs) but the CAR T-cells did not show any IONP internalization. Surprisingly, despite this lack of IONP internalization, it was found in preliminary experiments that the Si-IONP-loaded CAR T-cells were in fact magnetized, demonstrating that the Si-IONPs were associated with the CAR T-cells in some way (Supplementary Video 4). A closer examination of the TEM images consistently showed Si-IONPs aggregated in close proximity to the cell surface of CAR T-cells even after washing steps

to remove free particles, possibly suggesting some sort of non-specific association with the cell surface similar to the observations of Sanz-Ortega *et al*.[9] However, the precise mechanism of Si-IONP association with CAR T-cells is not known and will need to be thoroughly investigated before any therapeutic application. For the purposes of this proof-of-principle study of DPMF, though, we were satisfied with simply obtaining magnetized cells.

a)

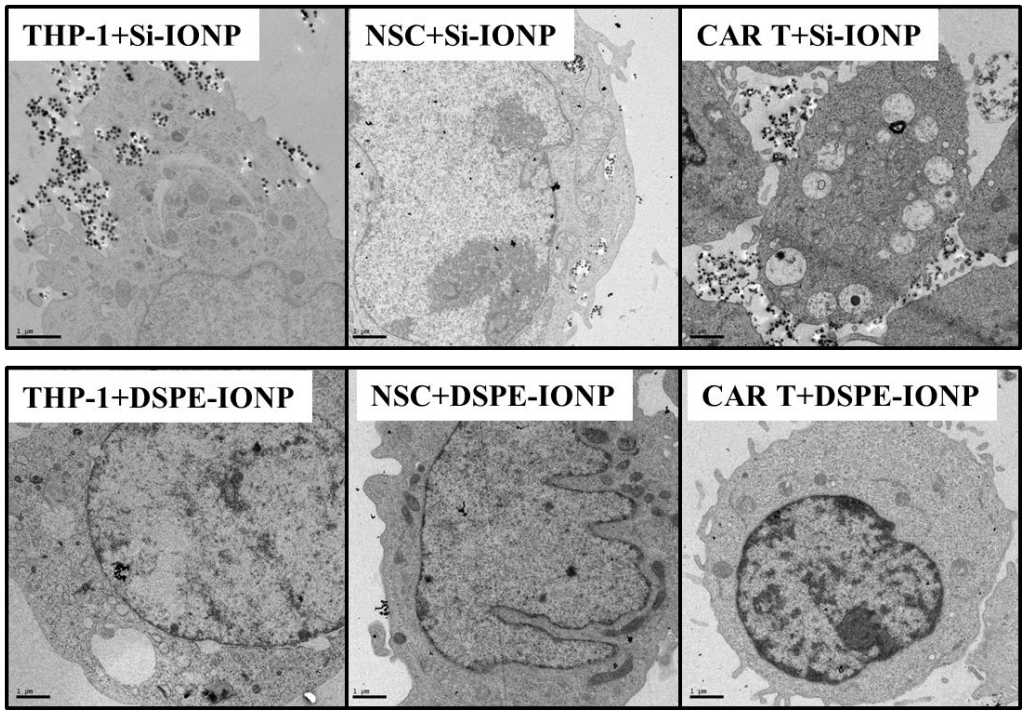
THP-1+Si-IONP
NSC+Si-IONP
CAR T+Si-IONP
THP-1+DSPE-IONP
NSC+DSPE-IONP
CAR T+DSPE-IONP

b)

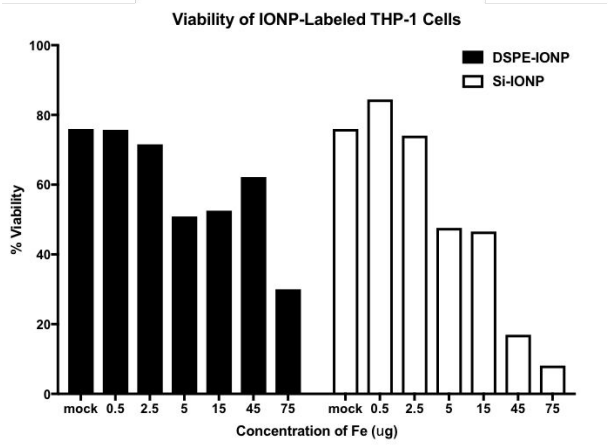
Viability of IONP-Labeled THP-1 Cells
DSPE-IONP
Si-IONP
% Viability
100
80
60
40
20
0
mock 0.5 2.5 5 15 45 75 mock 0.5 2.5 5 15 45 75
Concentration of Fe (ug)

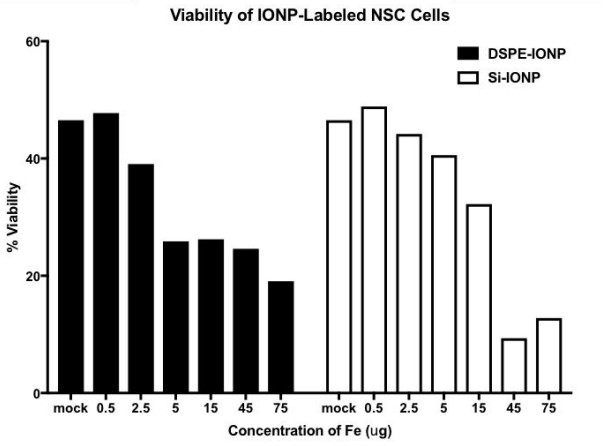
Viability of IONP-Labeled NSC Cells
DSPE-IONP
Si-IONP
% Viability
60
40
20
0
mock 0.5 2.5 5 15 45 75 mock 0.5 2.5 5 15 45 75
Concentration of Fe (ug)

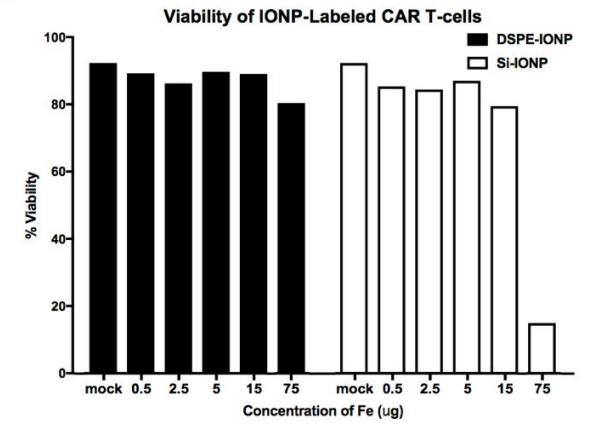
Viability of IONP-Labeled CAR T-cells
DSPE-IONP
Si-IONP
% Viability
100
80
60
40
20
0
mock 0.5 2.5 5 15 75 mock 0.5 2.5 5 15 75
Concentration of Fe (ug)

Figure 3. (a) TEM imaging of loaded cells. Cellular uptake and non-specific binding of Si-IONPs and DSPE-IONPs in cells. TEM images of Si-IONPs and DSPE-IONPs (IONPs with 10 μg of Fe content) labeled THP-1 cells, NSCs, and CAR T-cells. All scale bars are 1 μm. See Supplementary Figure 1 for additional TEM images of loaded cells. (b) Cell viability after loading with DSPE-IONP or Si-IONP.

Having identified the preferred IONP for loading each cell type, we proceeded to evaluate the ability of our DPMF chip to control the accumulation of the cells. For each cell type, the DPMF chip was initially programmed to target cells at one point (represented by the red dot in the box over the first arrows in Figure 4) and then after cells had accumulated at that position the chip was reprogrammed to target a second location (represented by the red dot in the box over the second arrows in Figure 4). Video was recorded for the entire duration of movement for each experiment (Supplementary Videos 2-4); only a representative sample of individual frames is presented in Figure 4. In the supplementary videos, it can be seen that the cells immediately change their trajectory when the target location is switched. It is evident from these observations as well as the positive control experiment involving the beads alone that the movement of the loaded cells is due to the magnetic field. To control for other non-magnetic causes of cell movement, cells alone (no IONP-loading) were exposed to the same DPMF focusing conditions. These negative controls showed no coordinated cell movement (data not collected). To serve as further validation, however, another negative control experiment showing no movement of loaded cells in the absence of a magnetic field is also provided for reference (Supplementary Video 5).

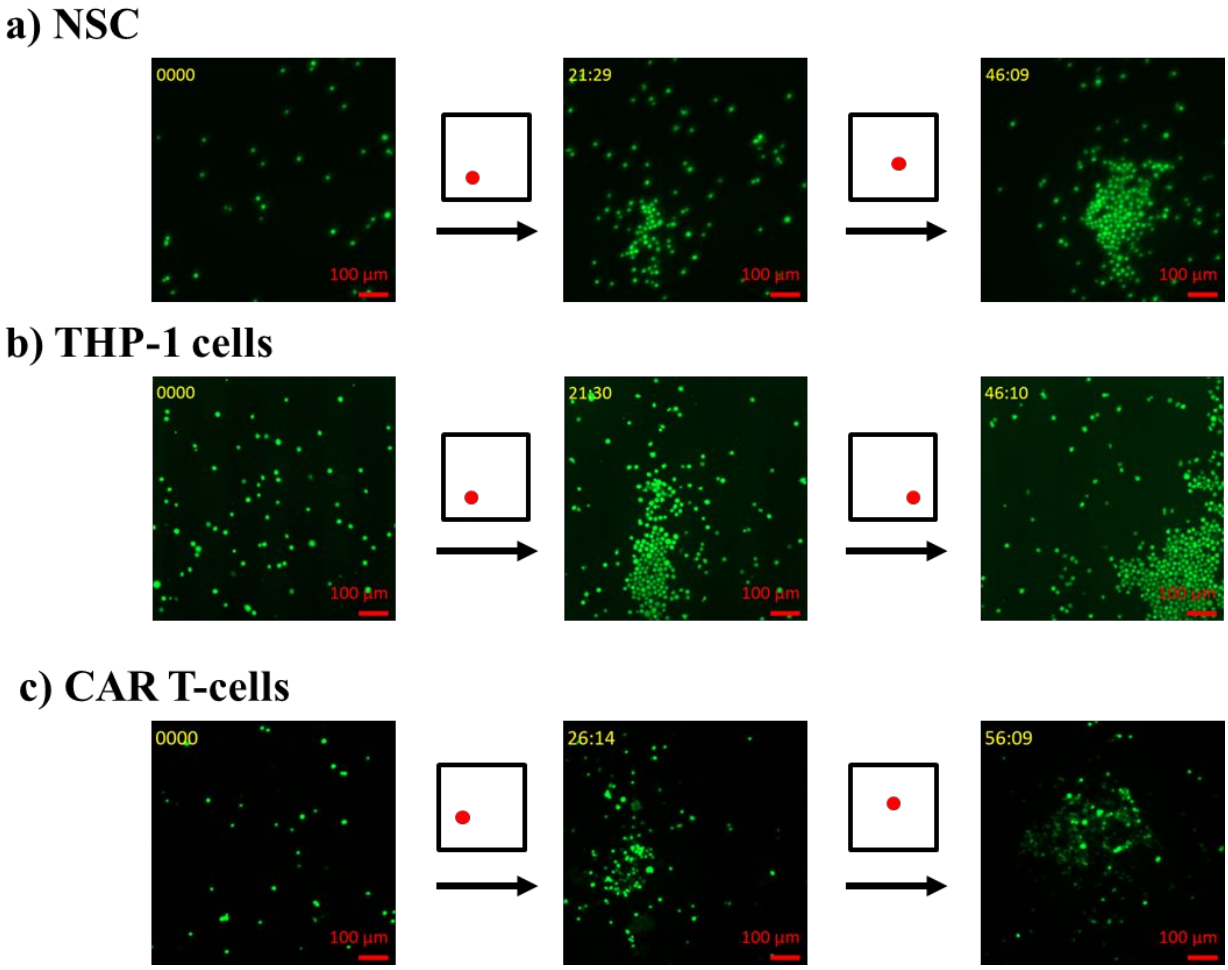

Figure 4. Magnetic movement of fluorescent cells controlled by DPMF. Each cell type is localized to an initial position, and then traversed to a secondary position. The localization positions are roughly indicated by the red dots. The final position of aggregation was deliberately changed during each experiment to showcase aggregation flexibility. (a) Magnetic movement of NSCs loaded with 0.5 µg of DSPE-IONPs. (b) Magnetic movement of THP-1 cells loaded with 0.5 µg of DSPE-IONPs. (c) Magnetic movement of CAR T-cells loaded with 30 µg of Si-IONPs. The cells are made fluorescent in the green channel by staining with CellTrace CFSE dye. The numbers in the top left corner of each image are the time stamps for that frame (mm:ss). To view the full original videos, see Supplementary Videos 2, 3, and 4, respectively.

An image processing algorithm was used to track cellular speeds during the DPMF experiments (Figure 5). Due to random variations in spatial distributions of cells, there is a large variation in the number of cells tracked for speed calculations. A total of 120 CAR T-cells, 390 THP-1 monocytes, and 230 NSCs were tracked. In general, cellular speed decreases as the cell moves closer to the aggregation point, as the magnetic force's in-plane (i.e., aggregating) component becomes weaker while its normal component becomes stronger. Reduction of speed also occurs because of cellular crowding. Note that there is more speed variability at farther radial distances due to the fact that the cells start from rest. Speeds of up to around 4.5 µm/sec were recorded at distances less than a millimeter away. On average, CAR T-cells tended to be the fastest,

whereas THP-1 cells exhibited the slowest movement. A two-sample unequal variances *t*-test was employed to establish the statistical significance of the observed deviations between the speeds of different cell types.[27, 28] Specifically, with a *p*-value not exceeding 0.05, both CAR T-cells and NSCs aggregated toward the center at least *twice* (or, more precisely, 2.2 times) as fast as the THP-1 cells did. Furthermore, at radial distances of 400 μm or greater, a comparison of CAR T-cells and NSCs revealed (again at a 5% significance level) that the average aggregation speeds of the CAR T-cells were higher by at least 18% or 0.4 μm/sec. On the other hand, note that differences in movement speeds among cells of the *same* type could be related to their hydrodynamic or adherent properties and/or variation in magnetic bead uptake. Overall, it was found that the movement of all three cell types loaded with two different IONP formulations could be readily controlled using the DPMF chip.

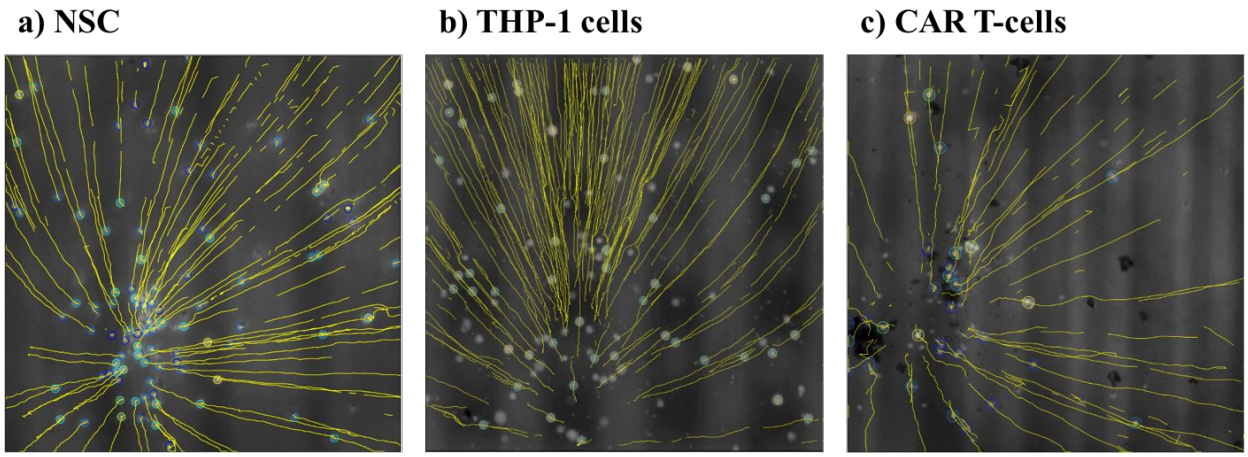

d)

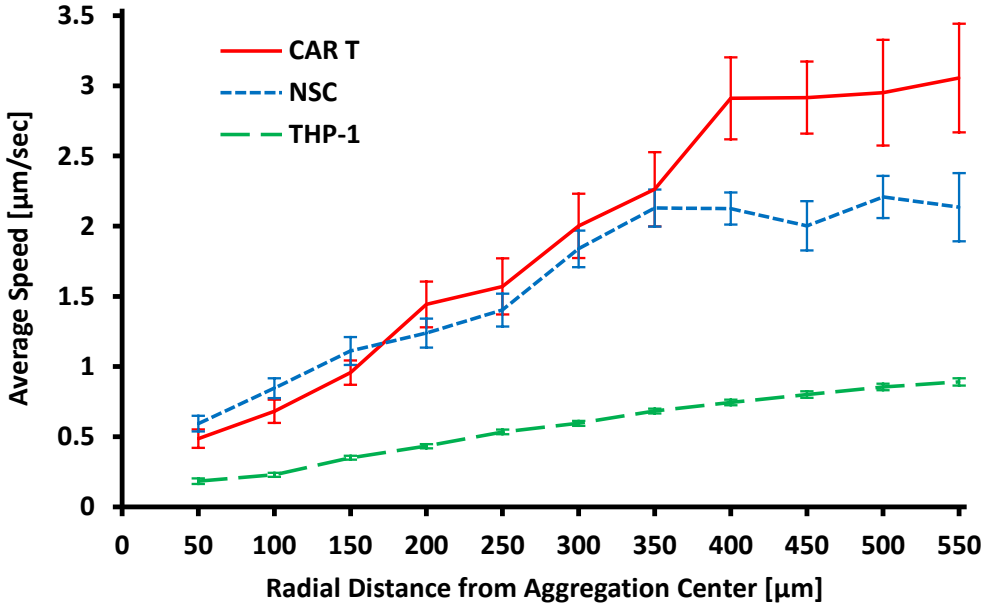

e)

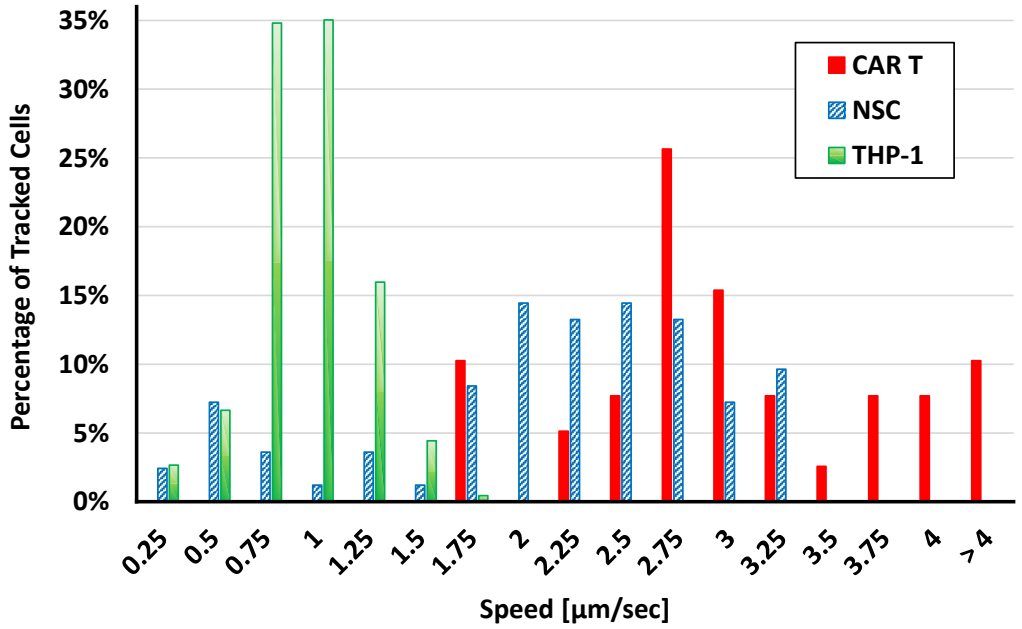

Figure 5. Cell tracking during DPMF. Cell trajectory contours (yellow lines) overlaid on a snapshot of the videos for (a) NSCs loaded with 0.5 µg of DSPE-IONPs, (b) THP-1 cells loaded with 0.5 µg of DSPE-IONPs, and (c) CAR T-cells loaded with 30 µg of Si-IONPs. The cells identified by the tracking algorithm are circled, where brighter colored circles indicate more clearly identified cells. In order to ensure a low false-positive rate for the tracking algorithm, not all cells in the video were successfully identified by the algorithm. (d) Average speeds of the tracked cells within a set of radial distance intervals (±10 µm of the axis labels). The error bars represent 95% confidence intervals for the average speeds. (The error bars for the THP-1 cells are barely noticeable.) (e) Distribution of speeds at a radial distance of 450 µm. Note that the speed-axis labels represent the *upper limits* of the bins.

CONCLUSION

We have demonstrated a prototype for DPMF-controlled cell movement. The current system is a miniature programmable electronic grid that can be rapidly reprogrammed in real time. We identified surface coatings for IONPs that facilitated loading of three different cell types used in cell therapies: stem cells (NSCs), macrophages (THP-1), and CAR T-cells. All of the loaded cells were readily controlled using the DPMF system, and this was visualized using our custom designed apparatus. While the current prototype is quite small and would not be used for human applications, the design can be directly scaled to larger formats to cover a sufficient therapeutic area. In addition, it is recognized that the forces exerted by the prototype are much too small to be effective in humans. However, the strength of the system will be dramatically boosted in future iterations by incorporating magnetizable materials that amplify the power of the programmable elements. The ability of DPMF to direct cell accumulation to an interior focal point combined with DPMF's inherent ability to be rapidly adjusted makes it a good candidate for applications in internal targeting for patients. In addition to creating a true aggregation point, DPMF may allow

for control of delivery paths throughout the body by adjusting fields to route particles along a desired trajectory.

MATERIALS AND METHODS

Instrumentation

Dynamic light scattering (DLS) and zeta potential (ZP) measurements were performed on a Brookhaven 90 Plus/BI-MAS Instrument (Brookhaven Instruments, New York). DLS measurements were obtained by performing 5 runs at 30 s per run and the ZP values by measuring 10 runs involving 20 cycles per run. All nanoparticle solutions were filtered through a 0.45 μm cellulose filter prior to performing DLS and ZP measurements.

Transmission electron microscopy (TEM) images were obtained with a with an FEI Tecnai T12 transmission electron microscope at an accelerating voltage of 120 keV and images were taken with a Gatan Ultrascan 2K CCD camera. NPs dispersed in water at an optimal concentration were drop cast onto glow-discharged, 300-mesh carbon/formvar coated grids and allowed to dry before imaging.

Materials

All organic and inorganic compounds (except PEG compounds) were purchased from Sigma Aldrich. 1,2-distearoyl-*sn*-glycero-3-phosphoethanolamine-N-[methoxy(polyethyleneglycol)-2000] (ammonium salt) (DSPE-PEG_{2000}) was purchased from Avanti Polar Lipids, Inc. (Catalogue #880120P). Super paramagnetic iron oxide nanoparticles suspended in chloroform (d = 30 nm, catalogue #SOR-30-50) were purchased from Ocean Nanotech, Springdale, AR, USA.

Cell Culture

All cells were cultured and maintained at 37°C in a humidified incubator (Thermo Electron Corporation, CA, USA) containing 5% CO_2. Neural stem cells were cultured in Dulbecco's Modifed Eagle's Medium (DMEM; Invitrogen, CA, USA) supplemented with 10% fetal bovine serum (Gemini Bio, CA, USA), 1% L-glutamine (Invitrogen) and 1% penicillin–streptomycin (Invitrogen). When the cells reached 80% confluency, they were passaged using a 0.25% trypsin/ethylenediaminetetraacetic acid solution (Invitrogen); media was changed every 2-3 days. THP-1 cells were cultured in RPMI 1640 medium (ATCC, USA) supplemented with 50 μM of β-mercaptoethanol, 10% fetal bovine serum (Gemini Bio, CA, USA), 1% L-glutamine (Invitrogen) and 1% penicillin–streptomycin (Invitrogen). THP-1 cell cultures were maintained at 2-8×10^5 viable cells/mL density by the addition of fresh medium or replacement of medium. CAR T-cells were obtained from Christine Brown (City of Hope, CA). Briefly, central memory subsets of CD3 T-cells were enriched and then transduced by lentivirus with an interleukin-13 (E13Y-mutated) ligand-based CAR, containing a 4-1BB costimulatory domain (IL13BBζ), and truncated CD19 (CD19t) as a marker for transduction efficiency. CAR T-cells were cultured in X-VIVO 15 medium supplemented with 10% fetal bovine serum (Gemini Bio, CA, USA). Cytokines IL2 and IL15 were added into cell culture three times a week.

Synthesis of DSPE-PEG coated Iron Oxide Nanoparticles (IONPs)

In a 20 mL scintillation vial, 1 mg of IONPs (40 μL, 25 mg/mL Fe) suspended in chloroform was added into 200 μL of chloroform, followed by the addition of excess of DSPE-PEG_{2000} (DSPE:IONP = 30:1 by weight) in 800 μL of chloroform. While the mixture was being

stirred at room temperature, DMSO (4 mL) was added into chloroform slowly, subsequently the mixture was shaken on a nutator for another 30 min. After chloroform being removed by reduced pressure, MilliQ water (16 mL) was added to the DMSO mixture dropwise to disperse the DSPE-PEG coated IONPs. DSPE-IONPs were washed with MilliQ water three times by centrifugation using a spin filter with a molecular weight cutoff of 100 kDa (3000 rpm, 1 min) and stored in MilliQ water at 4°C.

Synthesis of Silica-coated Iron Oxide Nanoparticles (Si-IONPs)

The preparation of silica-coated IONPs was adapted from the method reported previously by Lu *et al*.[29] In a 25-mL round bottom flask, 1 mg of IONPs (40 μL, 25 mg/mL Fe) suspended in chloroform was added into a mixture containing 7.7 mL cyclohexane, 2 mL Triton X-100, 1.6 mL hexanol, and 0.34 mL MilliQ water. The reaction mixture was stirred vigorously at room temperature for 5 min, and subsequently tetraethyl orthosilicate (TEOS, 40 μL) was added. The microemulsion system was further stirred at room temperature for 5 h before ammonium hydroxide (100 μL) was added to initiate the TEOS hydrolysis reaction. After stirring the reaction at room temperature for 24 h, the entire mixture was transferred to a 50 mL conical tube before being quenched with absolute ethanol (40 mL). Si-IONPs were collected by centrifugation (4000 rpm, 20 min) and washed three times by absolute ethanol with vortexing and sonication in between washes to help the NPs disperse back into solution.

Sample Preparation for Transmission Electron Microscopy (TEM)

Transmission electron microscopy (TEM) was performed on an FEI Tecnai 12 transmission electron microscope equipped with a Gatan Ultrascan 2K CCD camera. Cells labeled with DSPE-IONPs or SiIONPs described previously were collected by centrifugation, and washed once with PBS (500 g, 4 min). Cell pellets were then resuspended in fixative (2% glutaraldehyte in 0.1M Cacodylate buffer ($Na(CH_3)_2AsO_2 \cdot 3H_2O$), pH 7.2, at 4°C) overnight. The following day, cell pellets were washed three times with 0.1M Cacodylate buffer at pH 7.2, post-fixed with 1% OsO_4 in 0.1M Cacodylate buffer for 30 min, and washed three times with 0.1M Cacodylate buffer. The samples were then dehydrated step-wise via solvent exchange with 60%, 70%, 80%, 95% ethanol, 100% absolute ethanol (twice), propylene oxide (twice), and were left in propylene oxide/Eponate (1:1) overnight at room temperature in a sealed environment. The following day the vials were left opened at room temperature (~2-3 h) to allow propylene oxide to evaporate. The samples were then embedded in 100% Eponate with polymerization at ~64°C for 48 hours. Ultra-thin cell-containing sections (~70 nm thick) were cut using a Leica Ultra cut UCT ultramicrotome with a diamond knife, picked up on 200 mesh copper EM grids. Grids were stained with 2% uranyl acetate for 10 minutes followed Reynold's lead citrate staining for 1 minute.

In Vitro Cell Viability Assay by Flow Cytometry

THP-1 cells and NSCs were labeled with six doses of DSPE-IONPs and SI-IONPs cells containing 0.5, 2.5, 5, 15, 45, and 75 μg of Fe using the cell labeling method described above. After their exposure to various amount of IONPs for 1 h at 37°C, cells were washed once with PBS to remove unbound NPs, followed by staining with 1 mL of PBS containing 3 μM of propidium iodide for 15 min at room temperature. Their viability was then measured by flow cytometry.

Cell Box-Induced Cell Movement Captured by Live Cell Imaging

The cell box assembly was previously described by White *et al*.[17] Briefly, a large cover slip was attached onto the opening of a sterilized cell box using a non-cytotoxic silicone-based adhesive (Sibione Med Adhesive 4100 RTV, Factor II, Catalogue #A-4100). The adhesive was allowed to cure for 48 h at room temperature in a sterile environment (BS Level II hood). On the day of the cell box-induced cell movement experiments, THP-1 cells (1×10^7 cells) were cultured as described previously and labeled with DSPE-IONPs (0.5 μg of Fe per 1×10^6 NSC or THP-1 cells) or Si-IONPs (30 μg per 1×10^6 CAR T-cells) for 1 h at 37°C. The cells were also fluorescently labeled with CellTrace CFSE (per the manufacturer's instructions). After the exposure to IONPs, cells were washed once with PBS to remove unbound NPs before they were resuspended in full RPMI 1640 medium (10 mL) and transferred to a petri dish with a diameter of 100 mm. The box-coverslip assembly was inverted and submerged into the petri dish containing IONP-labeled cells in media. The experimental set up was enclosed in a glass chamber with regulated CO_2 level (5%). Live cell imaging was performed on a Zeiss Axio Observer Z1 inverted microscope with the Pecon/Zeiss incubation system. The camera and the microscope were controlled by the Zen Blue software. A bright-field picture was taken to indicate the initial location of the cells in solution under the view of the microscope after the cell box was set up on the microscope. The electric current in the wires in the magnetic grid was switched on to generate a magnetic field. Simultaneously, a video in the bright field channel was started to record the movement of the IONP-labeled cells in media under the cell box.

Dynamically-Programmable Magnetic Field (DPMF) Device

The DPMF apparatus (Figure 6) comprises three components: a controller, an inverted microscope, and a cell box. The controller is interfaced through a computer. The first system is a controller used to generate a particular magnetic field profile. The controller consists of a computer interface to a custom printed circuit board (PCB) constructed using a standard FR4 two-layer board. The PCB simultaneously controls 8 electromagnetic channels, each with a 16-bit current resolution and reversible polarity. A DAQ digital-to-analog converter (National Instruments, USA) is used to program voltage biases to the controller. Using a custom-developed software package, commands are input through the computer interface to dynamically program between various magnetic field profiles. The current setting is first regulated using a digital-to-analog converter. The analog signal is then buffered to a current source with a maximum swing of ±2 A, implemented using an integrated circuit operational amplifier connected in a feedback configuration via a PMOS transistor to a resistive load. The DPMF array features 300 μm traces at a pitch of 300 μm.

a)

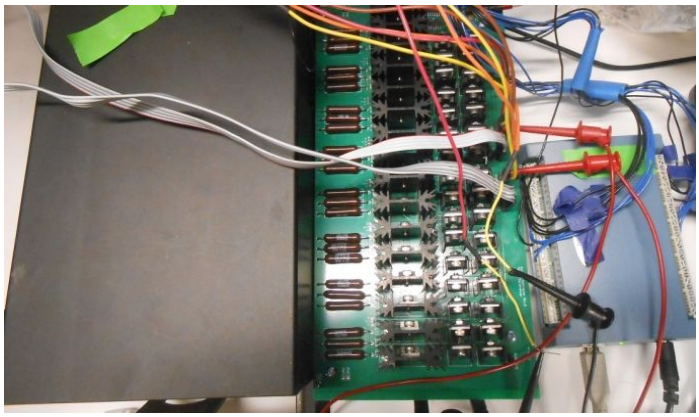

b)

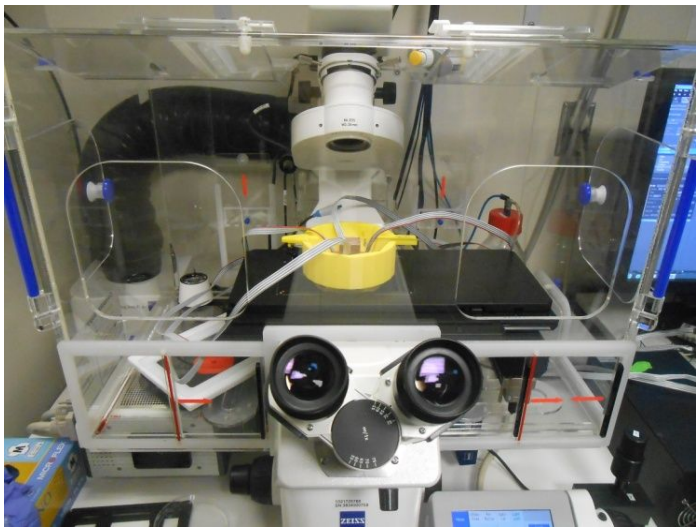

c)

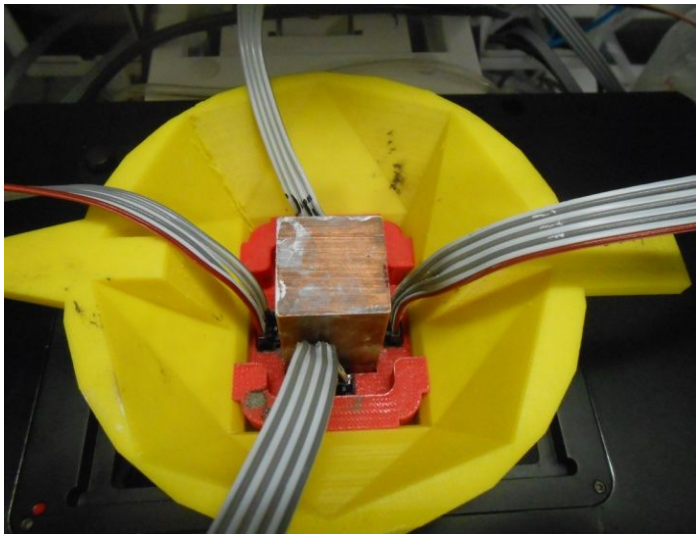

Figure 6. Measurement setup. (a) Circuitry responsible for individually addressing each wire consisting of a power supply, current controller, and digital-to-analog converter. (b) Cell box apparatus seated in inverted microscope. (c) Top view of cell box apparatus. Connectors interface directly to controller circuitry.

Next, the controller system interfaces with the second system, a cell box. The cell box design was previously described.[17, 26] The disposable cell box was printed using a Replicator 2 3D printer (Makerbot, USA) and is meant to interface the DPMF device with the microscope to enable live cell imaging of cell movement. To promote cell viability, it features an inlet port and distribution channels that interface with the microscope's incubation system to evenly distribute humidified CO_2 atmosphere in the petri dish. A pressure relief port prevents the accumulation of pressure and ensures a continuous flow of atmosphere. To reduce heating of the active area, a copper heatsink is placed on the current grid. A thin (25.4 mm × 25.4 mm × 0.1 mm) diamond sliver is placed between the heatsink along with thermal paste to help distribute heat to the heatsink.

Cell Speed Tracking

In order to track the cells and analyze their trajectories quantitatively, the videos demonstrating cell aggregation were analyzed using the TrackMate add-on in the image processing program ImageJ (Figure 5a-c). The speeds of the cells can be seen for each cell type (Figure 5d-e). A number of cells started from rest, as can be seen by some of the slower speed data points far away from the aggregation center. Due to crowding near the aggregation center, many cells stopped moving near 50 μm and were no longer successfully tracked at distances less than 50 μm.

ACKNOWLEDGMENTS

We gratefully acknowledge Marcia Miller, Zhuo Li, and Ricardo Zerda for electron microscopy performed in the EM core facility; Brian Armstrong, Loren Quintanar, and Tina Patel for their assistance with fluorescent imaging performed in the Light Microscopy and Digital Imaging Core. Research reported in this publication included work performed in the Electron Microscopy and the Light Microscopy and Digital Imaging Cores supported by the National Cancer Institute of the National Institutes of Health under award number P30CA033572. The content is solely the responsibility of the authors and does not necessarily represent the official views of the National Institutes of Health. The authors would like to thank R01CA155769, R21CA189223, R21 NS081594, NIH Grant 51013.914960.6692, The Kenneth T. and Eileen L. Norris Foundation and STOP Cancer for research funding.

SUPPORTING INFORMATION

Supplementary Figure 1 contains additional TEM images of loaded cells. Video 1 shows a positive control for movement of magnetic particles. Videos of cell aggregation are included for each of the cell types: neural stem cells (Video 2), THP-1 monocytes (Video 3), and CAR T-cells (Video 4). Video 5 shows a negative control for non-magnetic movement of cells related to the experimental setup. In this video, loaded CAR T-cells are used. These materials are available free of charge *via* the Internet at http://pubs.acs.org.

REFERENCES

1. Brown, C. E.; Badie, B.; Barish, M. E.; Weng, L.; Ostberg, J. R.; Chang, W.-C.; Naranjo, A.; Starr, R.; Wagner, J.; Wright, C.; Zhai, Y.; Bading, J. R.; Ressler, J. A.; Portnow, J.; D'Apuzzo, M.; Forman, S. J.; Jensen, M. C., Bioactivity and Safety of IL13Rα2-Redirected Chimeric Antigen Receptor CD8+ T Cells in Patients with Recurrent Glioblastoma. *Clin. Cancer Res.* **2015,** *21* (18), 4062-4072.

2. Cohn Yakubovich, D.; Sheyn, D.; Bez, M.; Schary, Y.; Yalon, E.; Sirhan, A.; Amira, M.; Yaya, A.; De Mel, S.; Da, X.; Ben-David, S.; Tawackoli, W.; Ley, E. J.; Gazit, D.; Gazit, Z.; Pelled, G., Systemic Administration of Mesenchymal Stem Cells Combined with Parathyroid Hormone Therapy Synergistically Regenerates Multiple Rib Fractures. *Stem Cell Res. Ther.* **2017,** *8* (51), 1-12.

3. Goldman, S. A., Stem and Progenitor Cell-Based Therapy of the Central Nervous System: Hopes, Hype, and Wishful Thinking. *Cell Stem Cell* **2016,** *18* (2), 174-188.

4. Newick, K.; O'Brien, S.; Moon, E.; Albelda, S. M., CAR T Cell Therapy for Solid Tumors. *Annu. Rev. Med.* **2017,** *68*, 139-152.
5. Palucka, K.; Banchereau, J., Dendritic-Cell-Based Therapeutic Cancer Vaccines. *Immunity* **2013,** *39* (1), 38-48.
6. Pernet, O.; Yadav, S. S.; An, D. S., Stem Cell-Based Therapies for HIV/AIDS. *Adv. Drug Delivery Rev.* **2016,** *103*, 187-201.
7. Portnow, J.; Synold, T. W.; Badie, B.; Tirughana, R.; Lacey, S. F.; D'Apuzzo, M.; Metz, M. Z.; Najbauer, J.; Bedell, V.; Vo, T.; Gutova, M.; Frankel, P.; Chen, M.; Aboody, K. S., Neural Stem Cell–Based Anticancer Gene Therapy: A First-in-Human Study in Recurrent High-Grade Glioma Patients. *Clin. Cancer Res.* **2017,** *23* (12), 2951-2960.
8. Telukuntla, K. S.; Suncion, V. Y.; Schulman, I. H.; Hare, J. M., The Advancing Field of Cell-Based Therapy: Insights and Lessons from Clinical Trials. *J. Am. Heart Assoc.* **2013,** *2* (5), 1-18.
9. Sanz-Ortega, L.; Rojas, J. M.; Marcos, A.; Portilla, Y.; Stein, J. V.; Barber, D. F. T Cells Loaded with Magnetic Nanoparticles Are Retained in Peripheral Lymph Nodes by the Application of a Magnetic Field. *J. Nanobiotechnol.* [Online], 2019. https://doi.org/10.1186/s12951-019-0440-z.
10. Burdick, J. A.; Mauck, R. L.; Gerecht, S., To Serve and Protect: Hydrogels to Improve Stem Cell-Based Therapies. *Cell Stem Cell* **2016,** *18* (1), 13-15.
11. Feyen, D. A. M.; Gaetani, R.; Doevendans, P. A.; Sluijter, J. P. G., Stem Cell-Based Therapy: Improving Myocardial Cell Delivery. *Adv. Drug Delivery Rev.* **2016,** *106*, 104-115.
12. Chen, A.; Byvank, T.; Chang, W.-J.; Bharde, A.; Vieira, G.; Miller, B. L.; Chalmers, J. J.; Bashir, R.; Sooryakumar, R., On-Chip Magnetic Separation and Encapsulation of Cells in Droplets. *Lab Chip* **2013,** *13* (6), 1172-1181.
13. Connell, J. J.; Patrick, P. S.; Yu, Y.; Lythgoe, M. F.; Kalber, T. L., Advanced Cell Therapies: Targeting, Tracking and Actuation of Cells with Magnetic Particles. *Regener. Med.* **2015,** *10* (6), 757-772.
14. Haisler, W. L.; Timm, D. M.; Gage, J. A.; Tseng, H.; Killian, T. C.; Souza, G. R., Three-Dimensional Cell Culturing by Magnetic Levitation. *Nat. Protoc.* **2013,** *8* (10), 1940-1949.
15. Ino, K.; Okochi, M.; Konishi, N.; Nakatochi, M.; Imai, R.; Shikida, M.; Ito, A.; Honda, H., Cell Culture Arrays Using Magnetic Force-Based Cell Patterning for Dynamic Single Cell Analysis. *Lab Chip* **2008,** *8* (1), 134-142.
16. Shen, Y.; Liu, X.; Huang, Z.; Pei, N.; Xu, J.; Li, Z.; Wang, Y.; Qian, J.; Ge, J., Comparison of Magnetic Intensities for Mesenchymal Stem Cell Targeting Therapy on Ischemic Myocardial Repair: High Magnetic Intensity Improves Cell Retention but Has No Additional Functional Benefit. *Cell Transplant.* **2015,** *24* (10), 1981-1997.
17. White, E. E.; Pai, A.; Weng, Y.; Suresh, A. K.; Van Haute, D.; Pailevanian, T.; Alizadeh, D.; Hajimiri, A.; Badie, B.; Berlin, J. M., Functionalized Iron Oxide Nanoparticles for Controlling the Movement of Immune Cells. *Nanoscale* **2015,** *7* (17), 7780-7789.
18. Muthana, M.; Kennerley, A. J.; Hughes, R.; Fagnano, E.; Richardson, J.; Paul, M.; Murdoch, C.; Wright, F.; Payne, C.; Lythgoe, M. F.; Farrow, N.; Dobson, J.; Connor, J.; Wild, J. M.; Lewis, C. Directing Cell Therapy to Anatomic Target Sites *In Vivo* with Magnetic Resonance Targeting. *Nat. Commun.* [Online], 2015. https://www.nature.com/articles/ncomms9009.
19. Jin, H.; Qian, Y.; Dai, Y.; Qiao, S.; Huang, C.; Lu, L.; Luo, Q.; Chen, J.; Zhang, Z., Magnetic Enrichment of Dendritic Cell Vaccine in Lymph Node with Fluorescent-Magnetic Nanoparticles Enhanced Cancer Immunotherapy. *Theranostics* **2016,** *6* (11), 2000-2014.
20. Polyak, B.; Medved, M.; Lazareva, N.; Steele, L.; Patel, T.; Rai, A.; Rotenberg, M. Y.; Wasko, K.; Kohut, A. R.; Sensenig, R., Magnetic Nanoparticle-Mediated Targeting of Cell Therapy Reduces In-Stent Stenosis in Injured Arteries. *ACS Nano* **2016,** *10* (10), 9559-9569.
21. Shapiro, B.; Depireux, D. A.; Sarwar, A.; Nacev, A.; Preciado, D.; Hausfeld, J., Pre-clinical Development of Magnetic Delivery of Therapy to Middle and Inner Ears. *ENT & Audiology News* **2014,** *23* (1), 54-56.

22. Nacev, A.; Komaee, A.; Sarwar, A.; Probst, R.; Kim, S. H.; Emmert-Buck, M.; Shapiro, B., Towards Control of Magnetic Fluids in Patients: Directing Therapeutic Nanoparticles to Disease Locations. *IEEE Control Syst. Mag.* **2012,** *32* (3), 32-74.
23. Nacev, A.; Weinberg, I. N.; Stepanov, P. Y.; Kupfer, S.; Mair, L. O.; Urdaneta, M. G.; Shimoji, M.; Fricke, S. T.; Shapiro, B., Dynamic Inversion Enables External Magnets to Concentrate Ferromagnetic Rods to a Central Target. *Nano Lett.* **2015,** *15* (1), 359-364.
24. Rosensweig, R. E., Heating Magnetic Fluid with Alternating Magnetic Field. *J. Magn. Magn. Mater.* **2002,** *252*, 370-374.
25. Beik, J.; Abed, Z.; Ghoreishi, F. S.; Hosseini-Nami, S.; Mehrzadi, S.; Shakeri-Zadeh, A.; Kamrava, S. K., Nanotechnology in Hyperthermia Cancer Therapy: From Fundamental Principles to Advanced Applications. *J. Controlled Release* **2016,** *235*, 205-221.
26. Pai, A.; Pailevanian, T.; White, E.; Dasgupta, K.; Sherman, J.; Alizadeh, D.; Cao, P.; Badie, B.; Hajimiri, A., Cell-Culturing, Imaging, and Magnetic Manipulation Using a Compact 3D Printed Chamber. In *Int. Conf. Miniaturized Syst. Chem. Life Sci., 19th*, Gyeongju, Korea, 2015; pp 600-602.
27. Welch, B. L., The Generalization of 'Student's' Problem When Several Different Population Variances Are Involved. *Biometrika* **1947,** *34* (1-2), 28-35.
28. Satterthwaite, F. E., An Approximate Distribution of Estimates of Variance Components. *Biom. Bull.* **1946,** *2* (6), 110-114.
29. Lu, C.-W.; Hung, Y.; Hsiao, J.-K.; Yao, M.; Chung, T.-H.; Lin, Y.-S.; Wu, S.-H.; Hsu, S.-C.; Liu, H.-M.; Mou, C.-Y.; Yang, C.-S.; Huang, D.-M.; Chen, Y.-C., Bifunctional Magnetic Silica Nanoparticles for Highly Efficient Human Stem Cell Labeling. *Nano Lett.* **2007,** *7* (1), 149-154.

TABLE OF CONTENTS GRAPHIC